

Protonic thermoelectric effect to superionic H₂O and magnetic field generation in Uranus and Neptune

Daohong Liu^{1,2}, Wei Zhang³, Yu He^{1,4,5,*}, Xinzhuan Guo^{1,4}, Chuanyu Zhang⁶, and Yang Sun⁷

¹*State Key Laboratory of Critical Mineral Research and Exploration,*

Institute of Geochemistry, Chinese Academy of Sciences, Guiyang 550081, China.

²*College of Earth and Planetary Sciences, University of Chinese Academy of Sciences, Beijing 100049, China.*

³*School of Geography and Environmental Science (School of Karst Science),*

Guizhou Normal University, Guiyang 550025, China.

⁴*Key Laboratory of High-Temperature and High-Pressure Study of the Earth's Interior,*

Institute of Geochemistry, Chinese Academy of Sciences, Guiyang 550081, Guizhou, China

⁵*Center for High Pressure Science and Technology Advanced Research, Shanghai 201203, China.*

⁶*College of Physics, Chengdu University of Technology, Chengdu, 610059, China.*

⁷*School of Materials, Sun Yat-sen University, Shenzhen, 518107, China.*

(Dated: March 3, 2026)

The origin of the anomalous magnetic fields of Uranus and Neptune, which exhibit significant tilts and multipolar configurations, is central to understanding the internal structure and evolution of the ice giants. Recent investigations confirmed that superionic H₂O ice is thermodynamically stable and constitutes the dominant H₂O phase within their icy mantles. Here, we use deep learning and *ab initio* molecular dynamics to investigate the thermal and protonic transport properties of the superionic H₂O ice. We demonstrate that the superionic H₂O ice exhibits a pronounced protonic thermoelectric effect, in which the maximum Seebeck coefficient within the interior of Uranus can reach $\sim 620 \mu\text{V}\cdot\text{K}^{-1}$, whereas that of Neptune is lower, within the range of $570\text{--}585 \mu\text{V}\cdot\text{K}^{-1}$. Consequently, the temperature gradients in the icy mantles can induce proton migration, which in turn drives magnetic field generation. Based on this mechanism, the disparities in magnetic field strength between Uranus and Neptune can be attributed to the differences in their internal temperature gradients, and the predicted magnitudes are in agreement with the results of observation from Voyager 2.

Unlike the predominantly dipolar and nearly axisymmetric magnetic fields of terrestrial planets and gas giants, the magnetic fields of Uranus and Neptune exhibit significant non-dipole and non-axisymmetric characteristics, with their magnetic axes substantially offset from the planetary center and highly inclined relative to the rotation axis [1–4]. This unique magnetic field configuration not only challenges conventional dynamo theory, but also offers critical insights into the internal dynamics, material states, and evolutionary history of the ice giants. To explain the anomalous geometry of magnetic fields of Uranus and Neptune, Stanley and Bloxham [5] proposed the thin-shell dynamo model. It posits that the magnetic field is generated within a relatively thin, convecting fluid layer in the outer part of the icy mantles, beneath which lies a large, stably stratified region. This thin-shell geometry produces smaller-scale convection, thereby generating a multipolar magnetic field. For the thin-shell dynamo model, whether a stable stratification can form beneath the convective layer, as well as the mechanical and electrical properties of the underlying stratification, are also key factors for the stable generation of magnetic fields [3]. Alternatively, the magnetic field may be generated by internal turbulence that is not strongly constrained by the planet's rotation [6], thus leading to a multipolar field. Nevertheless, the lack

of knowledge of the internal composition and transport properties of ice giants continues to impede our ability to discriminate among the magnetic field generation mechanisms and to identify the physical origin of the observed magnetic fields.

Interior structure models and high-pressure studies indicate that H₂O, CH₄, and NH₃ ices are the dominant components in the interior of Uranus and Neptune [7–19]. Besides, recent high-pressure experiments and theoretical calculations have confirmed the superionic transition of H₂O and NH₃ under the interiors of Uranus and Neptune [7–15, 17, 18]. In these superionic ices, protons diffuse like a liquid through solid-like sublattices of heavier nuclei. This unique phase simultaneously exhibits shear stiffness and extremely high ionic conductivity [20, 21]. In particular, superionic H₂O ice undergoes a structural transition from a body-centered cubic (bcc) to a face-centered cubic (fcc) phase with increasing temperature, accompanied by a significant increase in ionic conductivity [22]. The entropy contributed by the highly diffusive protons leads to high stability of the superionic fcc phase, which remains stable across most of the pressure-temperature (P-T) range of the icy mantles [8–10, 12, 14]. These findings imply that the superionic fcc H₂O ice is likely to be a major component of the icy mantles beneath the fluid H₂O layer. Therefore, its electrical and mechanical properties are proposed to influence the magnetic field generation in the ice giants [3, 20–25].

Ionic thermoelectric (*i*-TE) effect refers to a thermo-

* Email: heyu@mail.gyig.ac.cn

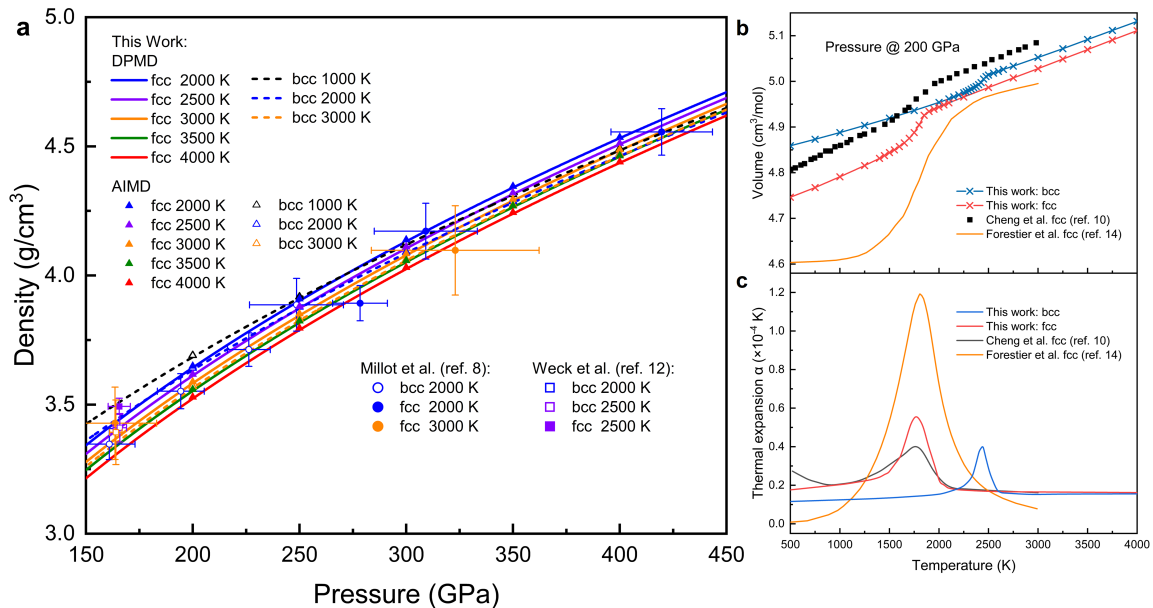


FIG. 1. Thermodynamic properties of bcc and fcc H_2O at 150–450 GPa and 2000–4000 K. **a**, Density-pressure relationships of the bcc and fcc H_2O at high P-T. The colors of the curves and symbols correspond to the magnitude of temperature along isotherms. Dashed and solid curves represent the DPMD calculation results for the bcc and fcc phases, respectively. Open and solid triangle symbols represent the AIMD calculation results. The previous experimental results are noted with circles and squares [8, 12]. **b**, Calculated molar volumes of bcc (blue cross-dotted line) and fcc (red cross-dotted line) are presented as a function of temperature along isobar at 200 GPa. A sharpening of the change in molar volume with increasing temperature suggests superionic transition. **c**, The volumetric thermal expansion coefficients are represented by blue and red curves for bcc and fcc H_2O in comparison with previous results [10, 14].

electric effect based on ionic transport [26–29], specifically a physical phenomenon wherein charged ions in ionic conductors (such as solid electrolytes, gels, ionic liquids, etc.) undergo directed migration driven by a definite temperature gradient, thereby establishing a thermovoltage across the material [27–29]. The *i*-TE materials, which present high Seebeck coefficients rivaling tens of $\text{mV}\cdot\text{K}^{-1}$, have been used for electric generation devices [26, 27, 30]. Since superionic H_2O ice is an effective proton conductor in the ice giants, the protonic thermoelectric (*p*-TE) mechanism might generate planetary-scale thermocurrents wherever a persistent thermal gradient exists. Such the thermocurrents would not merely be a passive product of interior dynamics but also influence the energy source and configuration of magnetic fields.

In this study, we calculated the protonic conductivity, thermal transport properties, and *p*-TE coefficients of superionic H_2O ice under the conditions of the interior of the ice giants using combined *ab initio* molecular dynamics (AIMD) and deep potential molecular dynamics (DPMD) methods. In addition, we also evaluated the potential impact of *p*-TE effect on planetary-scale magnetic field generation in Uranus and Neptune.

RESULTS

Density Profiles of Superionic H_2O Ice

We first evaluated our trained potential and computational method by comparing the pressure-temperature-density (P-T- ρ) relations of bcc and fcc H_2O calculated using AIMD and DPMD simulations at 150–450 GPa and 1000–4000 K, as shown in Fig. 1a. The density profiles of bcc and fcc H_2O calculated using DPMD show great agreement with AIMD results. The accuracy of the DP model was first assessed with *ab initio* validation datasets (Supplementary Fig. S1) and was further evaluated by comparing the predictions of radial distribution functions (RDFs) with AIMD results (Supplementary Figs. S2–S7). The calculated densities are also consistent with experimental results using static and dynamic compression methods [8, 12]. In addition, we found that fcc H_2O becomes denser than bcc H_2O at pressures above ~ 200 GPa (Fig. 1a), indicating that bcc H_2O becomes less compressible with increasing temperature. This behavior leads to the fcc phase exhibiting relatively significant compressibility and high stability in comparison with the bcc phase at high pressure, consistent with previous experimental results.

On the other hand, recent experimental studies have also emphasized the importance of volume expansion for

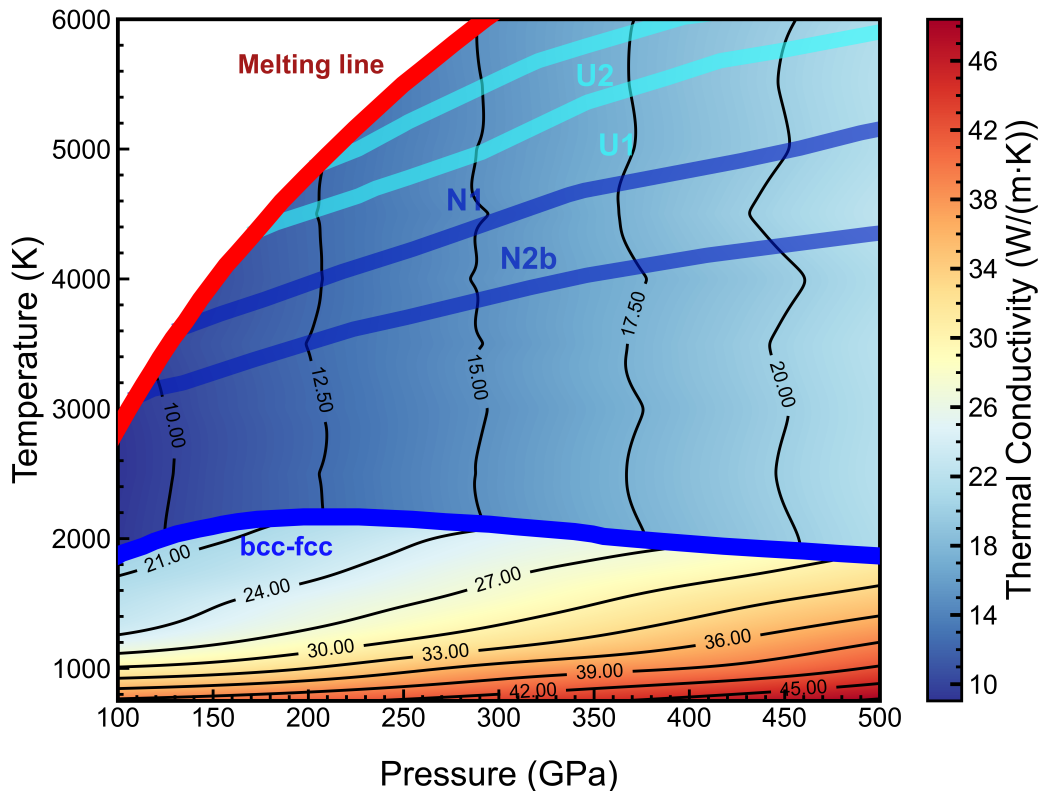


FIG. 2. **Thermal conductivity of bcc and fcc H_2O under conditions relevant to the interiors of Uranus and Neptune.** The contour lines indicate the magnitude of thermal conductivity. The blue and red curves exhibit the bcc-fcc and fcc-liquid phase boundary, respectively [15]. The cyan shaded band represents the U1 and U2 models, corresponding to the thermal profile of Uranus’s interior [32]. The dark blue shaded band represents the N1 and N2b models, corresponding to the thermal profile of Neptune’s interior [32].

the superionic transition of both bcc and fcc H_2O [14]. In this case, we determined the volume changes for bcc and fcc H_2O upon the superionic transition at 200 GPa with refined temperature intervals (Fig. 1b). Indeed, the onset of superionic state is accompanied with volume expansion. The superionic transition in bcc ice occurs at 2250–2600 K, which is ~ 500 K higher than the transition in fcc phase, consistent with experimental observation. The thermal expansion coefficients α (Fig. 1c), obtained from the fitted curves, exhibits a characteristic Λ -shaped peak associated with the onset of the superionic transition. The calculated peak value of α in this study is within the range of previous predictions [10, 14]. Our results have confirmed that the volume change upon the superionic transition is critical for the determination of the superionic transition temperature for experimental observations.

Thermal Transport and Protonic Thermoelectric of Superionic H_2O Ice

We calculated the thermal conductivity of bcc and fcc H_2O by employing the non-equilibrium molecular dy-

namics (NEMD) method (Supplementary Figs. S8–S11). In bcc H_2O , the thermal conductivity exhibits an obvious decrease with increasing temperature (Fig. 2 and Supplementary Fig. S12). This behavior can be attributed to intensified proton-phonon interactions driven by the superionic transition [31], which substantially shorten the phonon mean free paths (MFPs), thereby suppressing thermal transport. In contrast, the fcc H_2O exhibits a near temperature-independent lattice thermal conductivity, as shown in Supplementary Fig. S13. This apparent insensitivity to temperature stems from a distinct transport mechanism in which the thermal conductivity is governed by lattice phonons whose MFPs are primarily limited by proton-phonon scattering. Due to the extremely high diffusivity of protons in the superionic fcc phase, this scattering mechanism is intrinsically strong and nearly temperature-independent, resulting in a saturation of the phonon MFPs and a suppression of temperature-dependent effects. In addition, pressure has a monotonic enhancing effect on the thermal conductivity for both bcc and fcc H_2O . As pressure increases, atomic vibrations are increasingly constrained, reducing phonon scattering intensity and then promoting more efficient thermal transport. Based on the thermal profiles

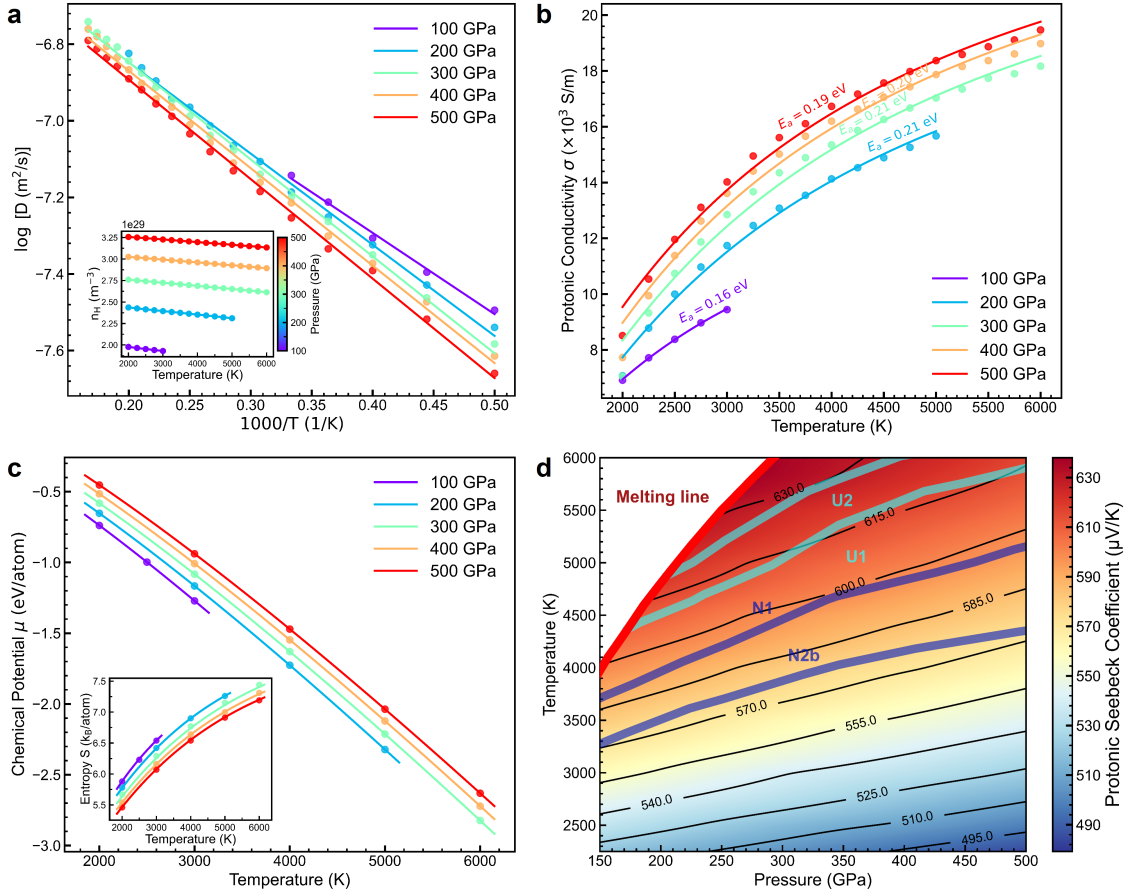


FIG. 3. **Protonic thermoelectric and transport properties of superionic fcc H₂O ice under the conditions relevant to the interiors of Uranus and Neptune.** **a**, The diffusion coefficient of proton was plotted as an Arrhenius equation with the relationship of $\log(D_H)$ vs. $1000/T$. The inset plot shows the number density of proton as a function of temperature at 100–500 GPa. **b**, Protonic conductivity of fcc H₂O with increasing temperature at 100–500 GPa. The E_a is the activation enthalpy, which exhibits negligible pressure dependence. **c**, Temperature dependence of chemical potential and the entropy (inset) for proton at 100–500 GPa. **d**, Pressure and temperature contour plot of the proton Seebeck coefficient with planetary thermal profiles (U1, U2 for Uranus and N1, N2b for Neptune) and the melting line highlighted [15, 32].

of Uranus and Neptune [32], H₂O mainly exists in the form of superionic fcc H₂O in icy mantles. The highly diffusive protons in fcc H₂O might lead to heat flux dissipation, thus decreasing the thermal conductivity efficiency in the interior of the ice giants.

We then calculated the temperature-dependent evolution of the protonic diffusion coefficient by fitting the mean-square displacements (MSDs) of protons under the internal P-T conditions relevant to Uranus and Neptune (Fig. 3a and Supplementary Figs. S14 and S15). The Nernst-Einstein equation is used to estimate the protonic conductivity of superionic fcc H₂O ice, and the protonic conductivity scatter plots are fitted using the Arrhenius equation, as presented in Fig. 3b. It is worth noting that the protonic conductivity of superionic fcc H₂O increases with rising pressure, which can be attributed to the increase in carrier (proton) concentration. Although the diffusion coefficient of proton decreases with pressure (Fig. 3a), the magnitude of the increase in proton

concentration exceeds the reduction in protonic diffusivity, leading to the enhancement of protonic conductivity (Fig. 3a inset).

Furthermore, to elucidate the thermoelectric response of superionic fcc H₂O, the Widom insertion method has been employed to compute the proton chemical potential, enabling us to determine the partial molar entropy of protons (Fig. 3c). Based on these values, we calculated the Seebeck coefficient of the superionic fcc H₂O within the framework of Onsager relations [26] under the interior conditions of Uranus and Neptune (Fig. 3d). The superionic fcc H₂O maintains a significant and relatively pressure-insensitive Seebeck response throughout the range of planetary interior conditions, underscoring the persistence of significant thermoelectric effect even in the deep interior of icy mantles. In the interior of ice giants, the Seebeck coefficient of fcc H₂O slightly increases with depth. The maximum Seebeck coefficient in Uranus can reach $620 \mu\text{V}\cdot\text{K}^{-1}$, while in Neptune, the coefficient

is lower, ranging between 570–585 $\mu\text{V}\cdot\text{K}^{-1}$.

Importantly, the high Seebeck coefficient is complemented by exceptional protonic conductivity, resulting in a large thermoelectric power factor, as shown in Supplementary Fig. S16. Quantitative comparison reveals that the power factor of superionic fcc H_2O surpasses that of many conventional ionic/electronic thermoelectric materials (Supplementary Fig. S17) [33, 34], suggesting that superionic fcc H_2O may constitute an efficient mechanism for energy conversion and charge redistribution in planetary interiors. These findings highlight the important role of superionic fcc H_2O in both magnetic field generation and heat dissipation in ice giants.

Geomagnetic fields generation in Uranus and Neptune

The highly eccentric and strongly non-dipolar magnetic field morphologies of Uranus and Neptune are thought to arise from a thin, active convective shell in their shallow interiors, overlain by a stable inner layer [55]. A key implicit premise of this model is that the thin shell must simultaneously possess sufficiently high electrical conductivity and intense turbulent convection to sustain an effective global dynamo process. Shock compression and computational results suggest the conductivity of fluid H_2O in the interiors of icy giants exceed ~ 1000 S/m [22, 35]. However, recent static conductivity measurements of dense fluid H_2O indicate that the fluid H_2O in the shallow thin layer, with a low conductivity of 10–40 S/m, cannot meet the requirement of a magnetic Reynolds number $R_m > 40$ [36]. Therefore, for the traditional dynamo to operate, it is necessary to assume that the internal temperature is several thousand Kelvin higher than that predicted by adiabatic models (approximately 4300 K), enabling H_2O to enter an electronically conducting state [36]. Nevertheless, according to the internal thermodynamic models of Uranus and Neptune [32, 37], such high temperatures are nearly unattainable in the shallow ionic fluid layer. Furthermore, recent observations and evolution models of ice giants have indicated that there are significant differences between the deep thermodynamic state and the full convection assumption of the dynamo model. Constraints from the interior structure and thermal evolution suggest that Uranus and Neptune may contain significant compositional gradients and thermal boundary layer structures [38–40], which might inhibit large-scale convection and result in a fainter radiated luminosity of Uranus [41]. On the other hand, numerical simulations also show that complex chemical mixtures may form stable stratified regions under high pressure, resulting in thermal transport efficiency lower than the model assumptions [4, 42].

Thermoelectric effect describes the direct conversion of heat into electricity without intense mechanical motion. This mechanism may become particularly significant for planets where low heat flux is insufficient to drive

the convection of conductive fluids [43]. Here, we found that superionic fcc H_2O , which occupies the icy mantles region above the rocky cores of Uranus and Neptune (Figs. 4a and 4b), presents significant the p -TE effect. Therefore, proton migration can be driven by the temperature gradient inside the ice giants. Based on proton convection induced by the steady-state temperature gradient across the adiabatic boundary layer, we utilized the Biot–Savart–Laplace law to calculate the planetary surface magnetic field strength under the p -TE conversion efficiency of 2.5%. By combining calculations of electrical conductivity along the internal thermal profiles of Uranus and Neptune, we fitted and annotated the contours of their internal protonic conductivity (σ) and temperature gradient ($\nabla_r T$) relationship in the diagram, as shown in Fig. 4c. The results indicate that within the estimated range for Uranus’s interior, the corresponding magnetic field strength values primarily fall near the 20–25 μT contour lines, which are in good agreement with the Uranus averaged surface magnetic field strength (23 μT) inverted by Voyager 2 [1]. On the other hand, the calculated magnetic field strength based on the σ - $\nabla_r T$ relation for Neptune is distributed between 15–20 μT and is also consistent with the observed average magnetic field strength of Neptune (13 μT) [2]. It is noteworthy that differences in the thermodynamic conditions of Uranus and Neptune produce distinct internal temperature gradients and electrical conductivity distributions, which in turn lead to the different magnetic field strengths, reflecting that Uranus can obtain a slightly higher average surface field strength than Neptune. This trend not only aligns with observations but also demonstrates that the thermoelectric circuit can naturally distinguish the magnetic field strengths of Uranus and Neptune.

The p -TE mechanism provides a new perspective on the origin of the magnetic fields in ice giants. This mechanism can be driven solely by internal temperature gradients, which does not require vigorous convective motions. Although p -TE can generate significant magnetic field strengths comparable to the observations, our calculation only considers the thermoelectric currents generated by a single component of fcc superionic H_2O . In reality, the true composition of the icy mantles might be mixed with complex ices such as NH_3 and CH_4 [17–19]. Recent studies also suggest possible reactions between H_2O and rocks to generate superionic hydrous phases [44]. This complex compositional heterogeneity leads to variations in local electrical and thermal conductivity, which in turn may cause variations of Seebeck coefficients in the icy mantles. In addition, lateral variations in temperature of the icy mantles may also lead to spatial fluctuations in the temperature gradient. The inhomogeneity caused by compositional differences and variations in temperature gradients in the icy mantles may affect the strength and direction of the p -TE current, resulting in spatially complex magnetic fields of Uranus and Neptune.

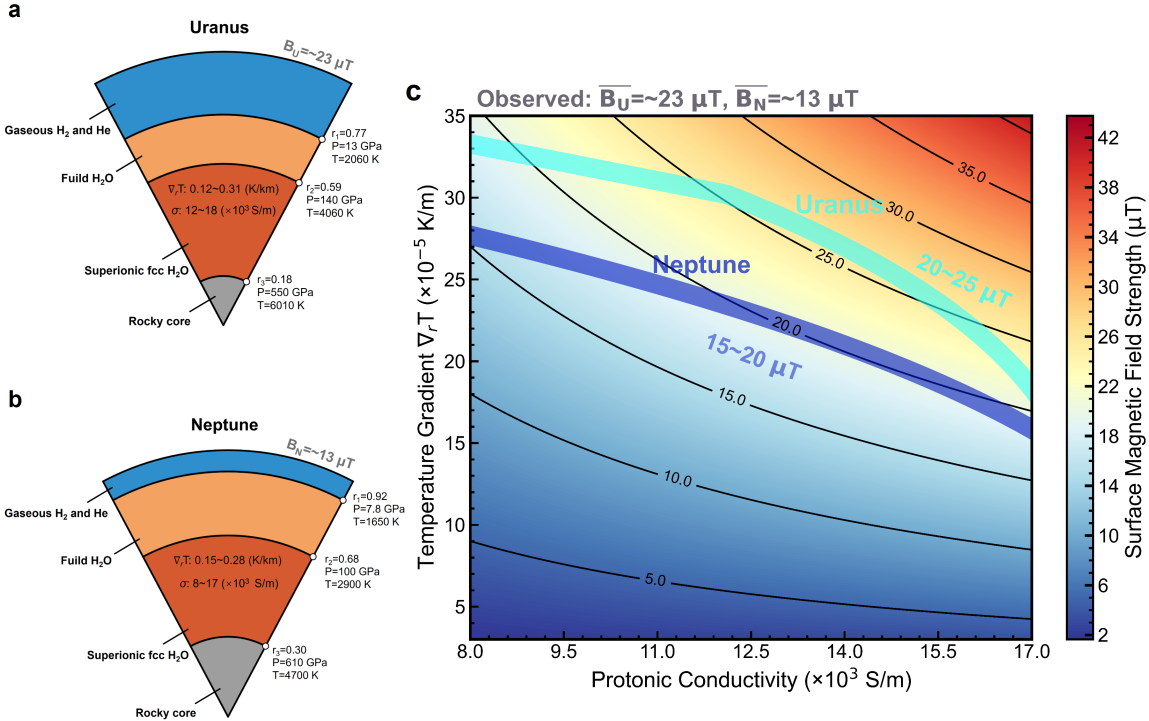


FIG. 4. The thermodynamic profiles of ice giants and the dependence of surface magnetic field strength on protonic conductivity and temperature gradient. **a**, Uranus' and **b**, Neptune's thermodynamic profiles of interior structures. **c**, The surface magnetic field strength as a function of protonic conductivity (σ) and radial temperature gradient ($\nabla_r T$) for the thermoelectric conversion efficiency of $\eta=2.5\%$. The cyan and dark blue shaded bands highlight the predicted surface magnetic field strength based on the σ and $\nabla_r T$ parameters of Uranus and Neptune. These regions present great consistency with the observed surface magnetic field strength of Uranus ($B_U \approx 23 \mu\text{T}$) and Neptune ($B_N \approx 13 \mu\text{T}$).

Acknowledgements The project is supported by National Key Research and Development Program of China, Grant No. 2024YFF0807500 (to Y.H.). We acknowledge the support of the National Natural Science Foundation of China, 42350002 (to Y.H.), the CAS Youth Interdisciplinary Team, JCTD-2022-16 (to Y.H.). Numerical computations were supported by the Open-Source Supercomputing Center of S-A-I.

Authors contribution Conceptualization: Y.H., Methodology: D.L., W.Z., Y.H., Y.S. Investigation:

D.L., Y.H. Visualization: D.L., C.Z. Funding acquisition: Y.H. Supervision: Y.H. Writing—original draft: D.L., Y.H. Writing—review & editing: D.L., W.Z., Y.H., X.G., C.Z., Y.S.

Competing interests The authors declare that they have no competing interests.

Data availability statement Data needed to evaluate the conclusions in the paper are present in the paper, and detailed methods of the calculations together with all necessary results are included in Supplementary Information at <http://xxx.xxx.xxx>.

- [1] N. F. Ness, M. H. Acuña, K. W. Behannon, L. F. Burlaga, J. E. Connerney, R. P. Lepping, and F. M. Neubauer, Magnetic fields at uranus, *Science* **233**, 85 (1986).
- [2] N. F. Ness, M. H. Acuña, L. F. Burlaga, J. E. Connerney, R. P. Lepping, and F. M. Neubauer, Magnetic fields at neptune, *Science* **246**, 1473 (1989).

- [3] R. Redmer, T. R. Mattsson, N. Nettelmann, and M. French, The phase diagram of water and the magnetic fields of uranus and neptune, *Icarus* **211**, 798 (2011).
- [4] K. Soderlund and S. Stanley, The underexplored frontier of ice giant dynamos, *Philosophical Transactions of the Royal Society A* **378**, 20190479 (2020).

- [5] S. Stanley and J. Bloxham, Convective-region geometry as the cause of uranus' and neptune's unusual magnetic fields, *Nature* **428**, 151 (2004).
- [6] K. Soderlund, M. Heimpel, E. King, and J. Aurnou, Turbulent models of ice giant internal dynamics: Dynamos, heat transfer, and zonal flows, *Icarus* **224**, 97 (2013).
- [7] M. Millot, S. Hamel, J. R. Rygg, P. M. Celliers, G. W. Collins, F. Coppari, D. E. Fratanduono, R. Jeanloz, D. C. Swift, and J. H. Eggert, Experimental evidence for superionic water ice using shock compression, *Nature Physics* **14**, 297 (2018).
- [8] M. Millot, F. Coppari, J. R. Rygg, A. Correa Barrios, S. Hamel, D. C. Swift, and J. H. Eggert, Nanosecond x-ray diffraction of shock-compressed superionic water ice, *Nature* **569**, 251 (2019).
- [9] J.-A. Queyroux, J.-A. Hernandez, G. Weck, S. Ninet, T. Plisson, S. Klotz, G. Garbarino, N. Guignot, M. Mezouar, M. Hanfland, *et al.*, Melting curve and isostructural solid transition in superionic ice, *Physical Review Letters* **125**, 195501 (2020).
- [10] B. Cheng, M. Bethkenhagen, C. J. Pickard, and S. Hamel, Phase behaviours of superionic water at planetary conditions, *Nature physics* **17**, 1228 (2021).
- [11] V. B. Prakapenka, N. Holtgrewe, S. S. Lobanov, and A. F. Goncharov, Structure and properties of two superionic ice phases, *Nature Physics* **17**, 1233 (2021).
- [12] G. Weck, J.-A. Queyroux, S. Ninet, F. Datchi, M. Mezouar, and P. Loubeyre, Evidence and stability field of fcc superionic water ice using static compression, *Physical Review Letters* **128**, 165701 (2022).
- [13] R. J. Husband, H. Liermann, J. McHardy, R. McWilliams, A. Goncharov, V. Prakapenka, E. Edmund, S. Chariton, Z. Konôpková, C. Strohm, *et al.*, Phase transition kinetics of superionic h₂o ice phases revealed by megahertz x-ray free-electron laser-heating experiments, *Nature communications* **15**, 8256 (2024).
- [14] A. Forestier, G. Weck, F. Datchi, S. Ninet, G. Garbarino, M. Mezouar, and P. Loubeyre, X-ray signature of the superionic transition in warm dense fcc water ice, *Physical Review Letters* **134**, 076102 (2025).
- [15] M. M. Raimondo Zavaroni, F. Matusalem, O. S. Cahuaranga Macollunco, J. Perretto Leandro, C. J. Ruestes, and M. de Koning, Phase behavior of a machine-learning potential trained on stress-strain curves: The case of superionic water ice, *The Journal of Chemical Physics* **163** (2025).
- [16] M. Podolak, A. Weizman, and M. Marley, Comparative models of uranus and neptune, *Planetary and Space Science* **43**, 1517 (1995).
- [17] C. Cavazzoni, G. Chiarotti, S. Scandolo, E. Tosatti, M. Bernasconi, and M. Parrinello, Superionic and metallic states of water and ammonia at giant planet conditions, *Science* **283**, 44 (1999).
- [18] J.-A. Hernandez, M. Bethkenhagen, S. Ninet, M. French, A. Benuzzi-Mounaix, F. Datchi, M. Guarguaglini, F. Lefevre, F. Occelli, R. Redmer, *et al.*, Melting curve of superionic ammonia at planetary interior conditions, *Nature Physics* **19**, 1280 (2023).
- [19] K. de Villa, F. González-Cataldo, and B. Militzer, Double superionicity in icy compounds at planetary interior conditions, *Nature Communications* **14**, 7580 (2023).
- [20] S. Sun, Y. He, D. Y. Kim, and H. Li, Anomalous elastic properties of superionic ice, *Physical Review B* **102**, 104108 (2020).
- [21] F. Matusalem, J. Santos Rego, and M. de Koning, Plastic deformation of superionic water ices, *Proceedings of the National Academy of Sciences* **119**, e2203397119 (2022).
- [22] M. French, S. Hamel, and R. Redmer, Dynamical screening and ionic conductivity in water from ab initio simulations, *Physical review letters* **107**, 185901 (2011).
- [23] E. Sugimura, T. Komabayashi, K. Ohta, K. Hirose, Y. Ohishi, and L. S. Dubrovinsky, Experimental evidence of superionic conduction in h₂o ice, *The Journal of chemical physics* **137** (2012).
- [24] F. Grasselli, L. Stixrude, and S. Baroni, Heat and charge transport in h₂o at ice-giant conditions from ab initio molecular dynamics simulations, *Nature Communications* **11**, 3605 (2020).
- [25] L. Stixrude, S. Baroni, and F. Grasselli, Thermal and tidal evolution of uranus with a growing frozen core, *The Planetary Science Journal* **2**, 222 (2021).
- [26] C.-G. Han, X. Qian, Q. Li, B. Deng, Y. Zhu, Z. Han, W. Zhang, W. Wang, S.-P. Feng, G. Chen, *et al.*, Giant thermopower of ionic gelatin near room temperature, *Science* **368**, 1091 (2020).
- [27] C. Chi, M. An, X. Qi, Y. Li, R. Zhang, G. Liu, C. Lin, H. Huang, H. Dang, B. Demir, *et al.*, Selectively tuning ionic thermopower in all-solid-state flexible polymer composites for thermal sensing, *Nature communications* **13**, 221 (2022).
- [28] N. Jabeen, M. Muddasar, N. Menéndez, M. A. Nasiri, C. M. Gómez, M. N. Collins, R. Muñoz-Espí, A. Cantarero, and M. Culebras, Recent advances in ionic thermoelectric systems and theoretical modelling, *Chemical Science* **15**, 14122 (2024).
- [29] O. Nickel, L. J. Ahrens-Iwers, R. H. Meißner, and M. Janssen, Water, not salt, causes most of the seebeck effect of nonisothermal aqueous electrolytes, *Physical review letters* **132**, 186201 (2024).
- [30] X. Qian, Z. Ma, Q. Huang, H. Jiang, and R. Yang, Thermodynamics of ionic thermoelectrics for low-grade heat harvesting, *ACS Energy Letters* **9**, 679 (2024).
- [31] N. I. Pavlenko and I. V. Stasyuk, The effect of proton interactions on the conductivity behavior in systems with superionic phases, *The Journal of Chemical Physics* **114**, 4607 (2001).
- [32] N. Nettelmann, R. Helled, J. Fortney, and R. Redmer, New indication for a dichotomy in the interior structure of uranus and neptune from the application of modified shape and rotation data, *Planetary and Space Science* **77**, 143 (2013).
- [33] A. Sohn and C. Yu, Ionic transport properties and their empirical correlations for thermal-to-electrical energy conversion, *Materials Today Physics* **19**, 100433 (2021).
- [34] S. Sun, M. Li, X.-L. Shi, and Z.-G. Chen, Advances in ionic thermoelectrics: from materials to devices, *Advanced Energy Materials* **13**, 2203692 (2023).
- [35] A. Mitchell and W. Nellis, Equation of state and electrical conductivity of water and ammonia shocked to the 100 gpa (1 mbar) pressure range, *The Journal of Chemical Physics* **76**, 6273 (1982).
- [36] K. Oka, Y. Okuda, and K. Hirose, Hot interiors of ice giant planets inferred from electrical conductivity of dense h₂o fluid, *arXiv preprint arXiv:2401.11454* (2024).
- [37] B. Militzer, Ab initio entropy calculations of water predict the interiors of uranus and neptune to be 15%–30% colder than previous models, *The Astrophysical Journal*

- 990**, 20 (2025).
- [38] S. Markham and D. Stevenson, Constraining the effect of convective inhibition on the thermal evolution of uranus and neptune, *The Planetary Science Journal* **2**, 146 (2021).
- [39] N. Nettelmann, K. Wang, J. J. Fortney, S. Hamel, S. Yellamilli, M. Bethkenhagen, and R. Redmer, Uranus evolution models with simple thermal boundary layers, *Icarus* **275**, 107 (2016).
- [40] M. Podolak, R. Helled, and G. Schubert, Effect of non-adiabatic thermal profiles on the inferred compositions of uranus and neptune, *Monthly Notices of the Royal Astronomical Society* **487**, 2653 (2019).
- [41] L. Scheibe, N. Nettelmann, and R. Redmer, Thermal evolution of uranus and neptune-ii. deep thermal boundary layer, *Astronomy & Astrophysics* **650**, A200 (2021).
- [42] H. Ravit, N. Nadine, and G. Tristan, Uranus and neptune: Origin, evolution and internal structure, *Space Science Reviews* **216** (2020).
- [43] A. N. Dmitriev, Thermoelectric currents of earth's core generate the earth's magnetic field, *International Journal of Geosciences* **8**, 1048 (2017).
- [44] S. Pan, T. Huang, A. Vazan, Z. Liang, C. Liu, J. Wang, C. J. Pickard, H.-T. Wang, D. Xing, and J. Sun, Magnesium oxide-water compounds at megabar pressure and implications on planetary interiors, *Nature Communications* **14**, 1165 (2023).